Up-converting nanoparticles synthesis using hydroxyl-carboxyl chelating agents: fluoride source effect

Ivana Dinic[1], Marina Vukovic[1], Marko Nikolic[2], Zhenquan Tan[3], Olivera Milosevic[4], Lidija Mancic[4*]

[1]Innovative Centre Faculty of Chemistry Belgrade, University of Belgrade, Serbia

[2]Photonic Center, Institute of Physics Belgrade, University of Belgrade, Serbia

[3]School of Petroleum and Chemical Engineering, Dalian University of Technology, China

[4]Institute of Technical Sciences of SASA, Belgrade, Serbia

[*]Corresponding autor: Liidja Mancic, lidija.mancic@itn.sanu.ac.rs

Abstract The synthesis of lanthanide doped up-converting nanoparticles (UCNPs), which morphological, structural and luminescence properties are well suited for application in optoelectronics, forensics, security or biomedicine, is of tremendous significance. Most commonly used synthesis method comprises decomposition of organometallic compounds in an oxygen-free environment and subsequent infliction of a biocompatible layer on particle surface. In this work, hydroxyl-carboxyl (-OH/-COOH) type of chelating agents (citric acid and sodium citrate) are used *in situ* for the solvothermal synthesis of hydrophilic $NaY_{0.5}Gd_{0.3}F_4$:Yb,Er UCNPs from rare earth nitrate salts and different fluoride sources (NaF, NH_4F and NH_4HF_2). The x-ray powder diffraction (XRPD) showed crystallization of cubic and hexagonal $NaY_{0.5}Gd_{0.3}F_4$:Yb,Er phase in nano and micro-sized particles respectively. Content of the hexagonal phase prevails in samples obtain when Na-citrate is used, while size and shape of synthesized mesocrystals is affected by the choice of fluoride source used for precipitation. All particles are functionalized with citrate ligands and emit intense green light at 519 and 539 nm ($^2H_{11/2}$,$^4S_{3/2}\rightarrow{}^4I_{15/2}$) under near infrared light. Intensity of this emission is distressed by the change of origin phonon energy of the host matrix revealed by change of the number of the excitation photons absorbed per emitted photon.

Keywords: up-conversion, $NaYF_4$**,** citrates, fluorides

1. Introduction

Lanthanide doped up-conversion nanoparticles (UCNPs) represent a promising material for miscellaneous application in optoelectronics, solar cells, security, forensics, bioimaging and drug delivery. [1-4] Following two or more excitation photons in the near infrared (NIR) wavelength range, UCNPs emit visible, UV or NIR light at shorter wavelength than excitation one on the account of a great difference in positions of the band maxima in their absorption and emission spectra (large Stokes shift). [5,6] The up-conversion (UC) efficiency and quantum yield depend on many factors, like choice of lanthanide dopants, their concentration ratio, crystal structure of matrix, etc.[7,8] The most commonly used lanthanide pairs for achieving efficient up-conversion comprise either ytterbium (Yb^{3+}) or neodymium (Nd^{3+}) as sensitizer, and erbium (Er^{3+}), holmium (Ho^{3+}) or thulium (Tm^{3+}) as activator.[9,10] Considering their partially occupied *4f* orbitals which are protected with outer *5s* and *5p* shells, lanthanides are capable to absorb the energy of NIR photons and emit light in visible spectra through establishing different energy transfer pathways. Among them energy transfer up-conversion (ETU) is considered to be the most efficient, due fact that absorption cross-section of the sensitizer is larger than that of the activator, so upon excitation of lower energy photons, both the sensitizer and the activator could be pumped to their excited states.[11] Subsequently, the sensitizer non-radiatively donates the energy to the activator via a dipole–dipole resonant interaction. Beside it, excited state absorption (ESA), photon avalanche (PA), cooperative energy transfer (CET), and energy migration-mediated up-conversion (EMU) could also contribute to the energy transfer in certain measure.[12] With regard to other inorganic hosts (like Y_2O_3 and Y_2O_2S), alkaline/rear earth fluorides (like $NaYF_4$ and YF_3) have proven to be better hosts for lanthanide doping, because of their higher refractive index and the lower phonon energy (≈ 350 cm^{-1}) which enhance the radiative emission rate, effectively reduce non-radiative energy losses at the intermediate states of lanthanide ions and consequently lead to a higher quantum yield.

Most widely studied $NaYF_4$ host crystallizes as cubic (α) or hexagonal (β) phase, whereby β phase shown to be more efficient in NIR-to-visible up-conversion. It is reported that visible UC emission of $NaYF_4$:Yb/Er microcrystals is 4.4 times higher in the hexagonal than that of cubic phase.[13] This is a consequence of the higher degree of crystal asymmetry and multisite occupation with dopants at shorter distance.[14-17] Production of the biocompatible monosized β-phased nanoparticles is under debate still, since well established procedure of organometalic precursors decomposition in a high-boiling organic solvent (oleic acid/oleylamine/octadecane), proposed initially by Mai et al.[18] yields hydrophobic nanoparticles so additional steps (like SiO2 encapsulation, ligand exchange/oxidation or polymer coating) are needed for achieving biocompatibility. Additionally, usage of hazardous substances during synthesis protocol applied raised deep concerns regarding potential toxicity of synthesized UCNPs.[19, 20] The solvothermal method is a more convenient and safe way to prepare biocompatible particles by changing the process parameters (temperature and reaction time) or precursor chemistry (including surfactants, chelating agents and solvents). [21, 22] To date, β-$NaYF_4$:Ln phase is stabilized in monosized nanoparticles when organic precursors such as trifluoracetates or stearates are solvothermaly treated.[23,24] Contrary, decomposition of inorganic chlorides and nitrates during hydrothermal processing usually guide to micro-sized particles growth, especially when EDTA or citric acid are used as chelating agents.[25-27] Addition of sodium citrate also stabilizes β phase in micro-crystals with various morphologies,[28, 29] while concurrent crystallization of α-$NaYF_4$:Ln phase is observed in the course of reaction time[27] or with increase of chelator to lanthanide molar ratio.[30] In this work, we investigated the influence of both, citric acid and sodium citrate, on the nucleation of β-$NaY_{0.5}Gd_{0.3}F_4$:Yb,Er phase during solvothermal synthesis. Effect of different precipitation agent i.e. fluorine source (NaF, NH_4F and NH_4HF_2) on the final particle morphology were also analyzed, due fact that cations derived from fluorine sources also play a role in growth of certain crystal facets. Partial substitution of yttrium by gadolinium is also performed, as suggested in[31], to promote further α to β

phase transition and intensify UC process. Under conditions explored here, stabilization of the well crystallized β-$NaY_{0.5}Gd_{0.3}Yb_{0.18}Er_{0.02}F_4$ phase with superior UC is enhanced when sodium citrate and ammonium fluoride are used during reaction.

2. Experimental

All of the chemicals used for citrate mediated hydrothermal synthesis of $NaY_{0.5}Gd_{0.3}Yb_{0.18}Er_{0.02}F_4$ were purchased from Sigma-Aldrich. Deionized water was used throughout. Defined stoichiometric amounts of rare earth nitrates (5 mmol in total) were dissolved initially in 3.5 ml of deionized water, and then mixed with 5 ml of citric acid (RE:cit=1:1) and 8.5 ml of NaF solution (RE:F=1:10). Afterwards, 34 ml of ethanol was added to the mixture, and pH value was adjusted to be 10 by adding a few drops of 0.1M NaOH. Obtained mixture was stirred for 15 min, and then transferred to 100 ml Teflon lined autoclave and sealed. Synthesis was carried out at temperature of 200 °C with a continual stirring (100 rpm) for 6 h. After cooling to the room temperature, the as-prepared powders were washed with water by centrifuging (7000 rpm, 5 min) and dried at 80 °C for 3 h. In the same way, the influence of various precipitation agents on the morphology of the particles, was analyzed using NH_4F and NH_4HF_2 (RE:F=1:10) with sodium citrate instead of citric acid (RE:cit=1:1). Nomenclature of the samples obtained was determined in accordance to the type of chelating agent and fluorine source used: Sample 1 (citric acid and NaF), Sample 2 (sodium citrate and NH_4HF_2) and Sample 3 (sodium citrate and NH_4F).

The phase composition of the as-prepared powders was determined by the X-ray powder diffraction (XRPD) using Rigaku SmartLab, equipped with a Cu-Kα source (λ= 1.5406 Å). The patterns were recorded with a step scan of 0.02° and accounting time of 2 s per step. Rietveld refinement of the structures was done in Topas 4.2 software using a Fundamental Parameter Approach.[32] Refinement of the cubic phase was carried out in *Fm-3m* (No. 225) space group, ICSD 60257, while for hexagonal phase P*63/m* (No. 176) ICSD 259189 was used. A predefined double-Voigt approach is used during isotropic size-strain

analysis, while ‘‘orientation distribution function” is included in fitting of diffraction lines intensities due to the observed preferential orientation. The particles morphological and structural properties were investigated by scanning electron microscopy (TESCAN VEGA 3 SB) and transmission electron microscopy (JEOL JEM 2100, operating at 200kV). Confirmation of the crystal structure in single particle was carried out using selected area electron diffraction (SAED). Chemistry of the surface was determined by Fourier transform infrared spectroscopy (FTIR) using Thermo Scientific Nicolet 6700 spectrophotometer with a Smart iTR Diamond Attenuated Total Reflectance accessory. Spectra were recorded using 128 scans at the resolution of 4 cm^{-1}. Photoluminescence spectra were measured at room temperature using Spex Fluorolog with C31034 cooled photomultiplier. For excitation we used CNI diode laser MDL-III-980-1W, at 980nm. UC intensity dependence on pump power was measured with Thorlabs power meter PM200 with S130C sensor. The sensor head was placed in front of the sample in the spectrometer. Power measurements were performed before and after luminescence intensity measurements.

3. Results and discussion

The XRPD patterns of $NaY_{0.5}Gd_{0.3}Yb_{0.18}Er_{0.02}F_4$ UCNPs presented in **Figure 1**, reflect that all samples obtained through hydrothermal treatment crystallize as a mixture of the particles with cubic ($NaYF_4$, space group Fm-3m, JCPDS file No.77-2042) and hexagonal ($NaYF_4$, space group P63/m, JCPDS 28-1192) phase. XRPD patterns of $NaY_{0.5}Gd_{0.3}Yb_{0.18}Er_{0.02}F_4$ UCNPs presented in **Figure 1**, reflect that all samples obtained through hydrothermal treatment crystallize as a mixture of the particles with cubic (space group *Fm-3m*, JCPDS file No.77-2042) and hexagonal (space group *P63/m,* JCPDS 28-1192) crystal arrangement. Since the Y^{3+} ions were substituted by larger Gd^{3+} ions in the host lattice, all diffraction peaks are lightly shifted to lower diffraction angles due to expansion of unit-cells. The fraction of hexagonal phase rises from 51.5 to 57.1 and then to 73.8 wt% (Sample 1, 2 and 3, respectively) with the change of chelating agents and fluoride source, **Table I**. Additionally, the diffraction peaks intensities

ratio of (110) and (101) planes changes in sample 3 in favor of former one, suggesting anisotropic c-axis growth of crystallites with a higher fraction of (001) packing planes. The size and microstrain of crystallites also changes, but with a different trend. The best crystallinity achieved in Sample 2 indicates that not only type of cations present from fluorine source, but also its excessive quantities, controls the morphology and crystal structure of both phases. When sodium is present in the excess during synthesis (Sample 1) binding of Na^+ ions to the citrate anions occur concurrently with the RE^{3+} chelating reactions contributing to kinetically induced nucleation of α-$NaY_{0.5}Gd_{0.3}Yb_{0.18}Er_{0.02}F_4$ phase. Contrary, when excess of NH_4^+ is present sufficiently long in the reaction mixture, nucleation of a thermodynamically stable hexagonal phase is enhanced. The difference between Samples 2 and 3 is content of NH_4^+ which is twice bigger in later one. Having in mind that citrate complexes formed through binding of trivalent ions comprise chelate rings with 7 and 8 members, while their counterparts generated through binding of ions of mixed valence have smaller rings of 5 members which are more stable thermodynamically [33, 34] it is logical to assume that formation of more stable citrate complex during synthesis of sample 3 contributes to the nucleation of β phase. It is worth to note that stabilization of β phase in the presence of the excess of Na^+ ions (due NaOH addition) is heavily reported in the literature[35] but in such cases nucleation of the hexagonal phase was induced by the change of pH which affects concentration of Y^{3+} and F^- in aqueous phase. In some cases, surplus of sodium could provoke NaF byproduct formation and subsequent growth of a large β-phase seeds from fluorine-deficient solution.[36]

Table I. Refined microstructural parameters of the $NaY_{0.5}Gd_{0.3}Yb_{0.18}Er_{0.02}F_4$ UCNPs

	Sample 1		Sample 2		Sample 3	
	α	β	α	B	α	β
Phase, mass%	48.5	51.5	42.9	57.1	26.2	73.8
a, Å	5.52920(7)	6.01774(42)	5.51546(3)	5.99946(16)	5.51471(12)	5.99301(9)
c, Å		3.54391(18)		3.53549(17)		3.53111(4)
CS, nm	84(5)	59(4)	169(3)	178(5)	35(1)	147(1)
Microstrain, %	0.207(15)	0.394(26)	0.038 (15)	0.0817(19)	0.134(7)	0.052 (1)

R_{wp}	4.141		5.41		4.645	
R_{Bragg}	3.15	1	6.96	1.91	3.11	1.54

Besides affecting nucleation, adsorption of citrate anions occurs onto different crystal planes of β phase nucleus, changing their relative surface energy and directing their further growth.[37] As it is shown in **Figure 2** all samples are composed from spherical α-phased nanoparticles and quite larger mesocrystals of β phase. Crystallization of spherical particles typically results in the formation of high packing-fraction structures such as *Fm-3m* face-centered cubic one. Since its isotropic unit cell induces growth of particles with a minimized surface energy of crystal facets, spherical morphology of the α $NaY_{0.5}Gd_{0.3}Yb_{0.18}Er_{0.02}F_4$ UCNPs stays unchanged with the change of the processing parameters in all samples. The particles mean size of about 100 (Sample 1), 200 (Sample 2) and 40nm (Sample 3) which corresponds well with a crystallites size determined through XRPD refinement implies their monocrystalline nature. The clear lattice fringes of (200) planes (2.75 Å, JCPDS 77-2042) are visible in **Figure 2(f)**. Contrary, SAED patterns of β phase mesocrystals, inset at **Figure 2(c),** shows the mixture of diffraction spots and rings confirming their polycrystalline structure. Calculated *d* spacing of 3.09, 2.14 and 1.54 Å correspond to (110), (201) and (112) crystal planes of β phase (JCPDS 28-1192), respectively.

This finding highlights that growth of such self-assembled morphology is based on intrinsically reconfigurable ability of α phased particles to pass barrier for the symmetry breaking and phase transition during solvothermal reaction. In contrast to that, presence of the sodium citrate during synthesis and its selective adsorption on certain crystal facets lead to the direct growth of anisotropic β phased mesocrystals.[27] As the growth went through a longer process hexagonal prisms and rods evolved by Ostwald ripening, as it was indicated by XRPD and microscopy analysis, **Figures 2(d,g)**. Thin enough to be transparent under the electron beam, these display an interplanar distance of (100) crystal plane, **Figures 2(h)**. Due to the presence of α phased spherical UCNPs on their surface, SAED pattern in **Figure 2(i)** can be indexed to (111) and (311) crystal planes of β phase and (220) and (222) crystal planes of α-phase.

In order to check retention of the chelating agents ligands at the particle surface, FTIR analysis was performed. Infrared absorption spectra of pure citric acid and sodium citrate are also presented in **Figure 3**. From comparison of the spectra, it is evident that free carboxylic acid groups (C=O stretching at 1754-1698 cm^{-1}) are not present in the samples, suggesting their coordination with metal ions on the particles surface.[38] Even more, band at 1580 cm^{-1} which is associated with antisymmetric C=O stretching vibration typical for sodium citrate is present in all samples, implicating that C=O bonding to sodium ion present at the particle surface. Also intensities of bands associated[30, 39, 40] with stretching vibration of –OH group at 3318-3008 cm^{-1}, CH_3 bending vibrations at 1417-1390 cm^{-1} and C-O stretching modes 1104 $cm^{-1}$are shifted and weakened (when compared to their original position) due change of their bond length. The most intense band associated with absorption of OH groups corresponds to spectrum of Sample 1, which shown weakest up-conversion emission.

The up-conversion spectra of $NaY_{0.5}Gd_{0.3}Yb_{0.18}Er_{0.02}F_4$ UCNPs under NIR light (980nm), show the presence of green and red Er^{3+} emissions, **Figure 4**. Green emission between 519 and 539 nm occurs from the $^2H_{11/2} \rightarrow {}^4I_{15/2}$ and $^4S_{3/2} \rightarrow {}^4I_{15/2}$ transitions, while a red emission observed between at 652 nm is due to the $^4F_{9/2} \rightarrow {}^4I_{15/2}$ transition.[41] It is notable that UC intensities rise with the increase of the hexagonal phase content in the samples. In the case of Yb^{3+}/Er^{3+} couple ground state absorption/excited state absorption (GSA/ESA) and energy transfer up-conversion (ETU) are two main mechanisms for UC process.[41] Later, which comprises numerous competing transitions between multiple energy levels is considered to contribute most. Thus under NIR photons Er^{3+} ion excites from the ground-state $^4I_{15/2}$ to the excited-state $^4I_{11/2}$ by one of the two following processes: ground-state absorption or energy transfer (ET) from the excited Yb^{3+} ions. Then, the ion in the $^4I_{11/2}$ state can be immediately excited to the $^4F_{7/2}$ level by absorbing another Yb^{3+} ion. The Er^{3+} ions could decay non-radiatively to the lower $^2H_{11/2}{}^4,S_{3/2}$, and $^4F_{9/2}$

levels enabling further their radiative transitions (i.e. green and red emission) to the ground $^4I_{15/2}$ level, **Figure 4(b)**. Since the lowest energy $^6P_{7/2}$ level of Gd^{3+} is located in ultraviolet region, it is not included in the up-conversion process.[31] The determined values of chromaticity coordinates which define the final light response of each sample are located in the green region of CIE diagram in **Figure 4(c).** The calculated intensity ratio of red to green emission is as follows: 0.86 (Sample1), 1.42 (Sample2) and 1.63 (Sample3). In the multiphoton absorption, the number of the photons (n) which take a part in the UC can be determined from the dependence of the emission intensity on the excitation power. Therefore, in order to analyze the energy transfer processes in samples UC intensity dependence on the pumping power is measured and presented in a log-normal plot, **Figure 5**. The logarithm of the UC emission intensity is linearly proportional to the pumping power with constant - n, which corresponds to the number of the excitation photons absorbed per emitted photon. Slope values of 1.53 ($^4S_{3/2} \rightarrow {}^4I_{15/2}$) and 1.50 ($^4F_{9/2} \rightarrow {}^4I_{15/2}$) for sample 2, and 1.61 ($^4S_{3/2} \rightarrow {}^4I_{15/2}$) and 1.58 ($^4F_{9/2} \rightarrow {}^4I_{15/2}$) for Sample 3 were obtained through fitting the data points presented in **Figure 5**. For both, green ($^4S_{3/2} \rightarrow {}^4I_{15/2}$) and red ($^4F_{9/2} \rightarrow {}^4I_{15/2}$) transitions two photons are involved in UC process, but higher values obtained for Sample 3 confirm that this sample is more efficient UC material. Weaker UC intensity of Sample 2 is associated with increased retention of surface ligands (detected by FTIR), which effect the origin phonon energy of the host matrix.

Conclusion

In summary, we have analyzed the coupled effect of different hydroxyl-carboxyl (-OH/-COOH) chelating agents and precipitation agents on the nucleation and growth of the hexagonal $NaY_{0.5}Gd_{0.3}Yb_{0.18}Er_{0.02}F_4$ UCNPs. Well crystallized mesocrystals of hexagonal phase were obtained when sodium citrate and

ammonium fluoride were used through *in situ* binding of ions of mixed valence and subsequent formation of more thermodynamically stable chelate rings. It was shown that shape and size of the mesocrystals are influenced by the choice of precipitation agents, while intensity of the green emission is governed by the change of origin phonon energy of the host matrix due retention of the hydroxyl and carboxyl groups at UCNPs surface.

Data Availability Statement:

The data that supports the findings of this study are available within the article.

Acknowledgements

This work was financially supported by the Ministry of Education, Science and Technological Development of Republic of Serbia, through Agreements related to the realization and financing of scientific research work of the Institute of Technical Sciences of SASA and Innovative Centre Faculty of Chemistry Belgrade in 2020, Contract numbers: 451-03-68/2020-14/200175 and 451-03-68/2020-14/200288.

References

1. D. Kumar, S.K. Sharma, S. Verma, V. Sharma, V. Kumar, "A Short Review on Rare Earth Doped $NaYF_4$ Upconverted Nanomaterials for Solar Cell Applications", Mater. Today: Proceedings 21, 1868–1874 (2020).
2. J. Yu, W. Yin,T. Peng, Y. Chang, Y. Zu, J. Li, X. He, X. Ma, Z. Gu,Y. Zhao, "Biodistribution, excretion, and toxicity of polyethyleneimine modified $NaYF_4$:Yb,Er upconversion nanoparticles in mice via different administration routes", Nanoscale 9, 4497 (2017).

3. X. Li, D. Zhao, F. Zhang, "Multifunctional Upconversion-Magnetic Hybrid Nanostructured Materials: Synthesis and Bioapplications", Theranostics 3 (5), 292–305 (2013).

4. Y. Han, H. Li, Y. Wang, Y. Pan, L. Huang, F. Song, W. Huang, "Upconversion Modulation through Pulsed Laser Excitation for Anti-counterfeiting", Sci. Rep. 7, 1320 (2017).

5. X. Zhu, Q. Su, W. Feng, F. Li," Anti-Stokes shift luminescent materials for bio-applications", Chem. Soc. Rev. 46, 1025-1039 (2017).

6. L. Zhao, A. Kutikov, J. Shen, C. Duan, J. Song, G. Han, "Stem Cell Labeling using Polyethylenimine Conjugated (α-$NaYbF_4$:Tm^{3+})/CaF_2 Upconversion Nanoparticles", Theranostics 3(4), 249-257 (2013).

7. S. Wang, A. Bi, W. Zeng, Z. Cheng, "Upconversion nanocomposites for photo-based cancer theranostics"**,** J. Mater. Chem. B 4, 5331-5348 (2016).

8. H. Dong, L.-D. Sun, C.-H. Yan, "Energy transfer in lanthanide upconversion studies for extended optical applications", Chem. Soc. Rev. 44, 1608-1634 (2015).

9. X. Liang, J. Fan, Y. Wang, Y. Zhao, R. Jin, T. Sun, M. Cheng, X. Wang, "Synthesis of hollow and mesoporous structured $NaYF_4$:Yb,Er upconversion luminescent nanoparticles for targeted drug delivery", J. Rare Earth. 35 (5), 419 (2017).

10. L. Marciniak, M. Stefanski, R. Tomala, D. Hreniak, W. Strek, "Synthesis and up-conversion luminescence of Er^{3+} and Yb^{3+} codoped nanocrystalline tetra- ($KLaP_4O_{12}$) and pentaphosphates (LaP_5O_{14})", J. Chem. Phys. 143, 094701 (2015).

11. H. Dong, L.-D. Sun, C.-H. Yan, "Energy transfer in lanthanide upconversion studies for extended optical applications", Chem. Soc. Rev. 44, 1608-1634 (2015).

12. F. Auzel, "Upconversion and Anti-Stokes Processes with f and d Ions in Solids ", Chem. Rev. 104, 139-173 (2004).

13. A.Kar, S. Kundu, A. Patra, "Lanthanide Doped Nanocrystals: Strategies for Improving the Efficiency of Upconversion Emission and Their Physical Understanding ", ChemPhysChem, 16, 505-521 (2015).

14. F. Wang, X. Liu, "Recent advances in the chemistry of lanthanide - doped upconversion nanocrystals", Chem. Soc. Rev. 38 (4), 976 – 989 (2009).

15. T. Laihinen, M. Lastusaari, L. Pihlgren, L. C. V. Rodrigues, J. Holsa, "Thermal behaviour of the $NaYF_4:Yb^{3+},R^{3+}$ materials", J. Therm. Anal. Calorim. 121, 37–43 (2015).

16. C. Li, J. Lin, "Rare earth fluoride nano-/microcrystals: synthesis, surface modification and application", J. Mater. Chem. 20, 6831–6847 (2010).

17. G. Pawlik, J. Niczyj, A. Noculak,2 W. Radosz, A. Podhorodecki, "Multiband Monte Carlo modeling of upconversion emission in sub 10 nm β-$NaGdF_4:Yb^{3+}$, Er^{3+} nanocrystals—Effect of Yb^{3+} content", J. Chem. Phys. 146, 244111 (2017).

18. H.-X. Mai, Y.-W. Zhang, R. Si, Z.-G. Yan, L.-D. Sun, L.-P. You, C.-H. Yan, "High-Quality Sodium Rare-Earth Fluoride Nanocrystals: Controlled Synthesis and Optical Properties" , J. Am. Chem. Soc. 128, 6426–6436 (2006).

19. X. Wu, G. Chen, J. Shen, Z. Li, Y. Zhang, G. Han, "Upconversion nanoparticles: a versatile solution to multiscale biological imaging" , Bioconjug. Chem. 26 , 166−175 (2015).

20. G.K. Das, D.T. Stark, I.M. Kennedy, "Potential toxicity of up-converting nanoparticles encapsulated with a bilayer formed by ligand attraction", Langmuir 30, 8167–8176 (2014).

21. W. L. Suchanek, R. E. Riman, "Hydrothermal Synthesis of Advanced Ceramic Powders", Adv. Sci. Tech. 45, 184-193 (2006).

22. I.Z. Dinic, M. E. Rabanal, K. Yamamoto, Z. Tan, S. Ohara, L. T. Mancic, O. B. Milosevic," PEG and PVP assisted solvothermal synthesis of $NaYF_4:Yb^{3+}/Er^{3+}$ up- conversion nanoparticles", Adv. Powder Technol. 27, 845-853 (2016).

23. H.-Q. Wang, T. Nann, "Monodisperse Upconverting Nanocrystals by Microwave-Assisted Synthesis", ACS Nano. 3 (11), 3804–3808 (2009).

24. M. Wang, C.-C. Mi, J.-L. Liu, X.-L. Wu, Y.-X. Zhang, W. Hou, F. Li, S.-K. Xu, "One-step synthesis and characterization of water-soluble NaY_{F4}:Yb,Er/Polymer nanoparticles with efficient up-conversion fluorescence", J. Alloys Compd. 485, L24–L27 (2009).

25. I. Z. Dinic, L. T. Mancic, M. E. Rabanal, K. Yamamoto, S. Ohara, S. Tamura, T. Koji, A. M. L. M. Costa, B. A. Marinkovic, O. B. Milosevic, "Compositional and structural dependence of up-converting rare earth fluorides obtained through EDTA assisted htdro/solvothermal synthesis", Adv. Powder Technol. 28, 73-82 (2017).

26. R. Zhou, T. Ma, B. Qiu, X. Li, "Controlled synthesis of β-$NaYF_4$:Yb, Er microphosphors and upconversion luminescence property", Mater. Chem. Phys. 194, 23-28 (2017).

27. C. Li, Z. Quan, J. Yang, P. Yang, J. Lin, "Highly Uniform and Monodisperse α- $NaYF_4:Ln^{3+}$ (Ln) Eu, Tb, Yb/Er, and Yb/Tm Hexagonal Microprism Crystals: Hydrothermal Synthesis and Luminescent Properties", Inorg. Chem. 46, 6329-6337 (2007).

28. M. Ding, S. Yin, Y. Ni, C. Lu, D. Chen, J. Zhong, Z. Ji, Z. Xu, "Controlled synthesis of α-$NaYF_4:Yb^{3+}/Er^{3+}$ microstructures with morphology-and size-dependent upconversion luminescence", Ceram. Int. 41, 7411-7420 (2015).

29. W. Shan, R. Li, J. Feng, Y. Chen, D. Guo, "Hydrothermal synthesis and up-conversion luminescence of $NaYF_4:Yb^{3+},Tm^{3+}$ phosphors", Mater. Chem. Phys. 162, 617-627 (2015).

30. T. Jiang, W. Qin, W. Di, R. Yang, D. Liu, X. Zhai, G. Qin, "Citric acid-assisted hydrothermal synthesis of α- $NaYF_4$:Yb^{3+},Tm^{3+} nanocrystals and their enhanced ultraviolet upconversion emissions", Cryst .Eng. Comm. 14, 2302-2307 (2012).

31. F. Wang, Y. Han, C. S. Lim, Y. Lu, J. Wang, J. Xu, H. Chen, C. Zhang, M. Hong, X. Liu, "Simultaneous phase and size control of upconversion nanocrystals through lanthanide doping ", Nature, 463, 1061–1065 (2010).

32. TOPAS, General Profile and Structure Analysis Software for Powder Diffraction Data; V4.2, Bruker AXS GmbH, Karlsruhe, Germany

33. P. Caravan, J. J. Ellison, T. J. McMurry, R. B. Lauffer, "Gadolinium(III) Chelates as MRI Contrast Agents: Structure, Dynamics, and Applications", Chem. Rev. 99, 2293−2352 (1999).

34. M. Matzapetakis, C. P. Raptopoulou, A. Tsohos, V. Papaefthymiou, N. Moon, A. Salifoglou, "Synthesis, spectroscopic and structural Characterization of the first mononuclear, water soluble iron−citrate complex, $(NH_4)_5Fe(C_6H_4O_7)_2{\cdot}2H_2O$", J. Am. Chem. Soc. 120 (50), 13266-13267 (1998).

35. C. Wang, X. Cheng, "Controlled hydrothermal growth and tunable luminescence properties of β-$NaYF_4$:Yb^{3+}/Er^{3+} microcrystals", J. Alloys Compd. 617, 807–815 (2014).

36. H. Li, L. Xu, G. Chen,"Controlled Synthesis of Monodisperse Hexagonal $NaYF_4$:Yb/Er Nanocrystals with Ultrasmall Size and Enhanced Upconversion Luminescence", Molecules, 22, 2113 (2017).

37. C. Li, J. Yang, Z. Quan, P. Yang, D. Kong, J. Lin,"Different Microstructures of α-NaYF4 Fabricated by Hydrothermal Process: Effects of pH Values and Fluoride Sources", Chem. Mater. 19, 4933-4942 (2007).

38. M. Pedroni, F. Piccinelli, T. Passuello, S. Polizzi, J. Ueda, P. Haro-Gonzalez, L. Martinez Maestro,D. Jaque, J. García-Sole, M. Bettinelli, A. Speghini," Water (H_2O and D_2O) Dispersible

NIR-to-NIR Upconverting Yb^{3+} /Tm^{3+} Doped MF_2 (M = Ca, Sr) Colloids: Influence of the Host Crystal ", Cryst. Growth Des. 13, 4906−4913 (2013).

39. L. C. Bichara. H. E. Lanus, E. G. Ferrer, M. B. Gramajo, S. A. Brandan, "Vibrational Study and Force Field of the Citric Acid Dimer Based on the SQM Methodology", Adv. Phys. Chem. 347072, 1-10 (2011).

40. N. C. Dyck, F. C. J. M. van Veggel, G. P. Demopoulos, "Size-Dependent Maximization of Upconversion Efficiency of Citrate- Stabilized β-phase $NaYF_4$:Yb^{3+},Er^{3+} Crystals via Annealing", ACS Appl. Mater. Interfaces 5, 11661−11667 (2013).

41. S. Heer, K. Kompe, H. -U. Gudel, M. Haase, "Highly efficient multicolour upconversion emission in transparent colloids of lanthanide-doped $NaYF_4$ nanocrystals", Adv. Mater. 16 (23-24), 2102-2105 (2004).

The Journal of Chemical Physics

Figure captions:

FIG. 1. (a) XRD pattern of $NaY_{0.5}Gd_{0.3}Yb_{0.18}Er_{0.02}F_4$ UCNPs, and Rietveld refinement of samples: (b) Sample 1, (c) Sample 2, (d) Sample 3.

FIG. 2. SEM /TEM/HRTEM and SAED images of: (a-c) Sample 1, (d-f) Sample 2, (g-i) Sample 3.

FIG. 3. FTIR analysis of $NaY_{0.5}Gd_{0.3}Yb_{0.18}Er_{0.02}F_4$ UCNPs and hydroxyl-carboxyl chelating agents used during their synthesis

FIG. 4. (a) Up-converted spectra of $NaY_{0.5}Gd_{0.3}Yb_{0.18}Er_{0.02}F_4$ UCNPs excited at 980 nm, (b) corresponding energy level diagram of Yb^{3+}, Er^{3+} and Gd^{3+} dopants and (c) CIE diagram

FIG. 5. UC emission intensity dependence on the pumping power (a) Sample 2 (b) Sample 3

PLEASE CITE THIS ARTICLE AS DOI: 10.1063/5.0016559

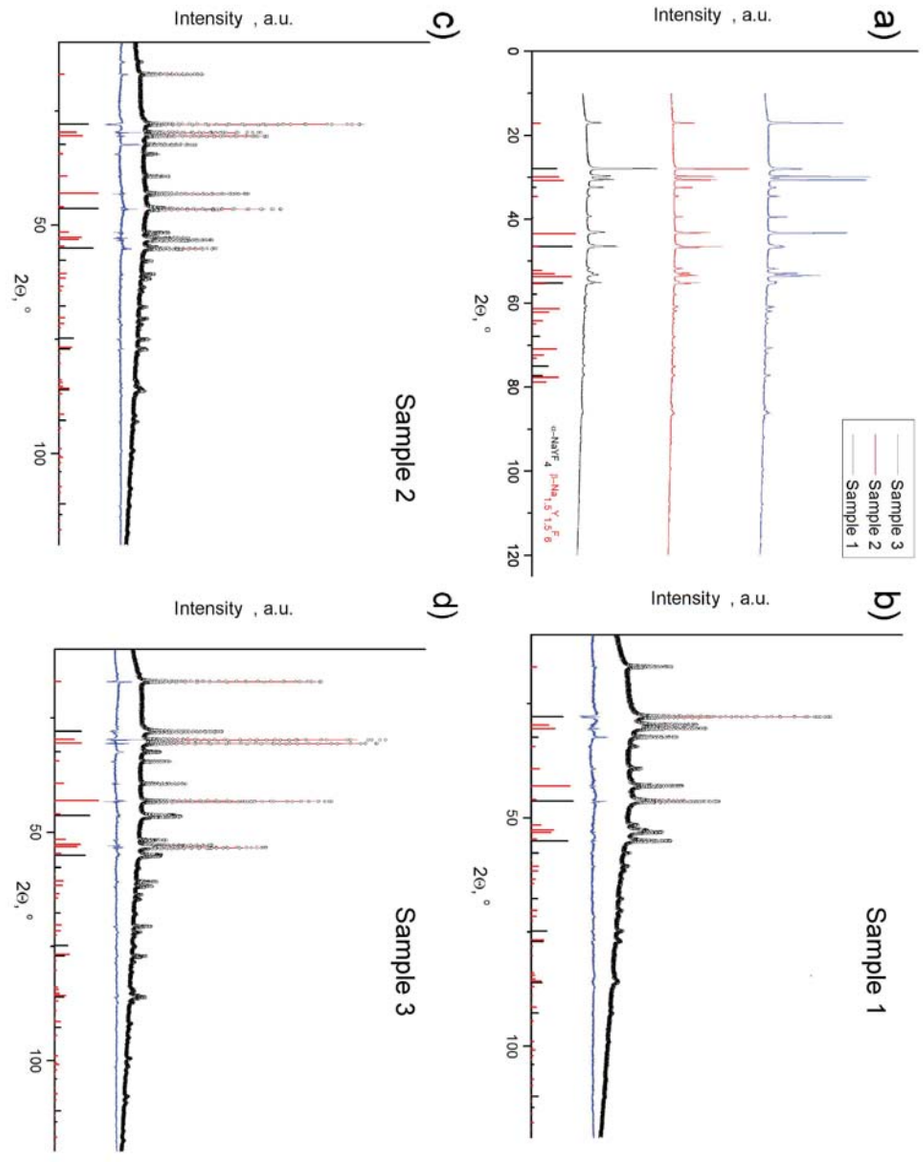

AIP Publishing

The Journal of Chemical Physics

ACCEPTED MANUSCRIPT

PLEASE CITE THIS ARTICLE AS DOI: 10.1063/5.0016559

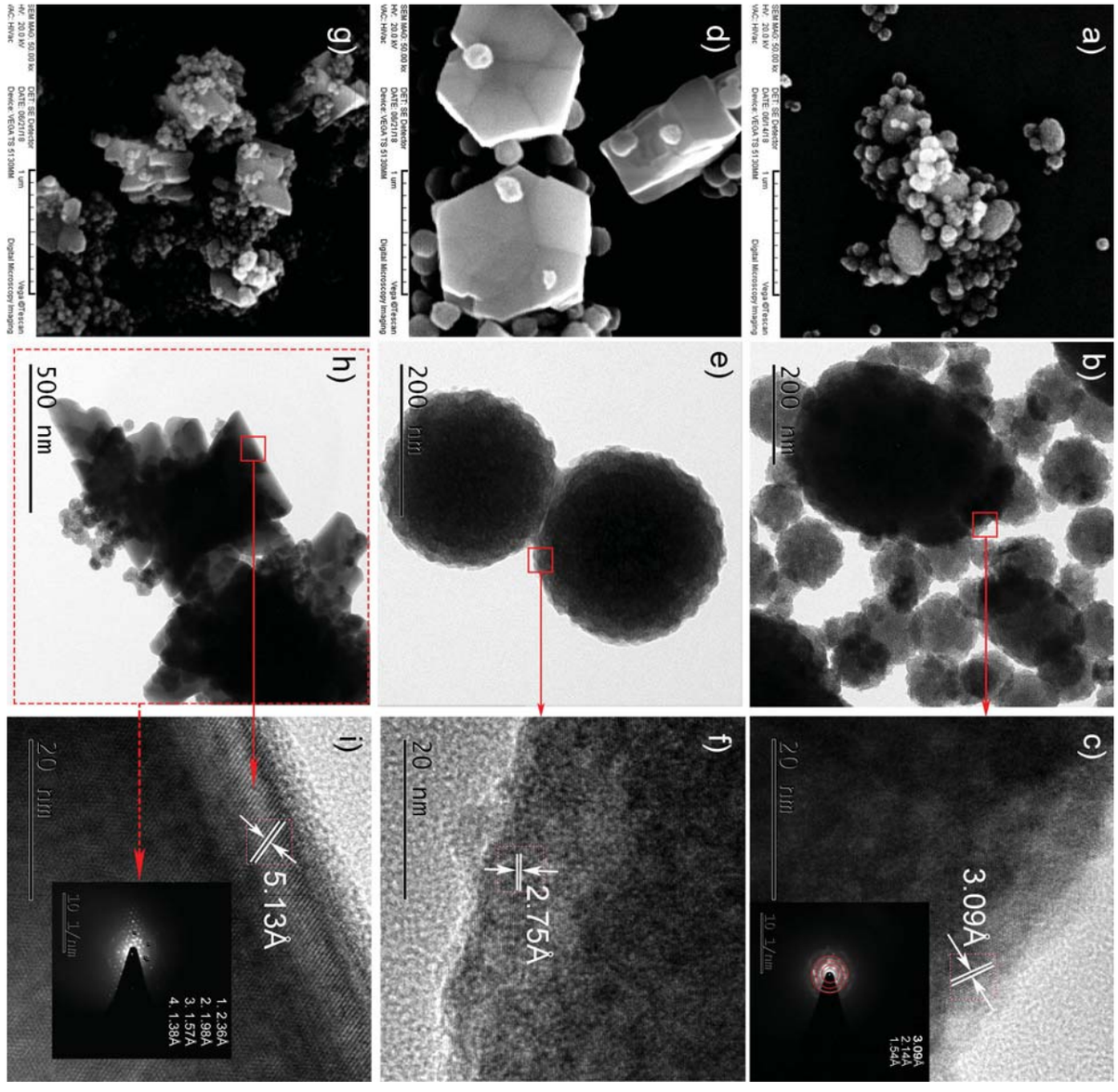

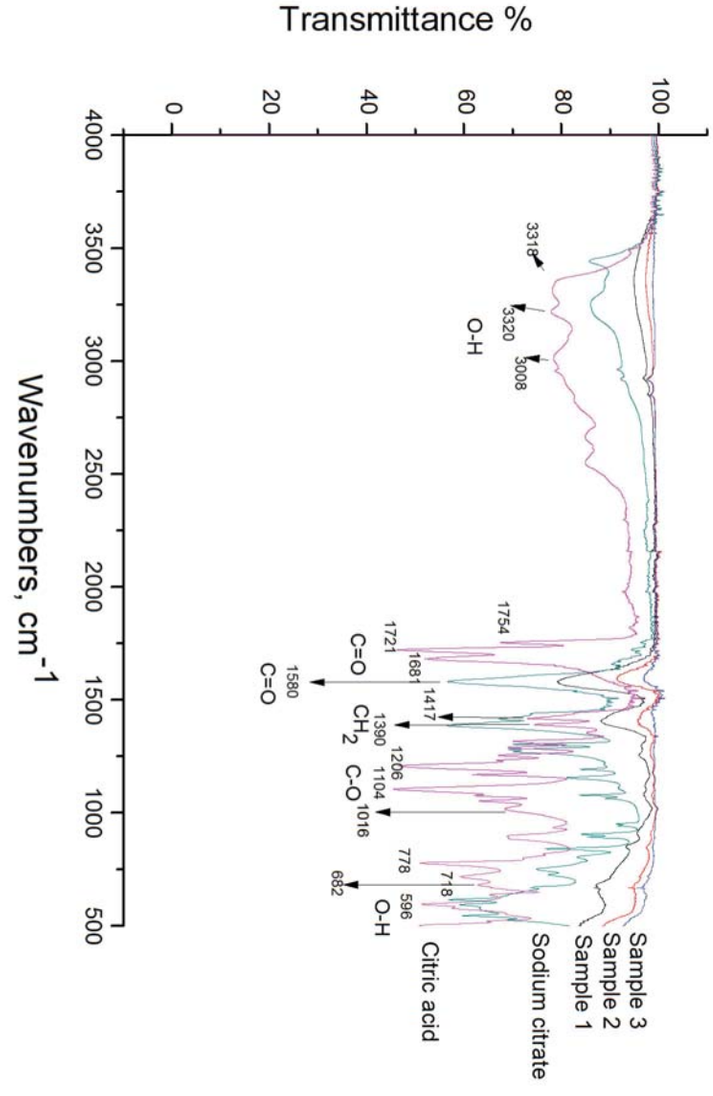

The Journal of Chemical Physics

PLEASE CITE THIS ARTICLE AS DOI: 10.1063/5.0016559